A comparison of entrainment velocity and displacement speed statistics in different regimes of turbulent premixed combustion

Nilanjan Chakraborty[1*], Markus Klein[2], Hong G. Im[3]

[1]School of Engineering
University of Newcastle
Claremont Road, Newcastle
NE1 7RU, UK
Email: nilanjan.chakraborty@ncl.ac.uk

[2]Bundeswehr University Munich, Department of Aerospace Engineering, LRT1,
Werner-Heisenberg-Weg 39, 85577 Neubiberg, Germany
Email: markus.klein@unibw.de

[3]Clean Combustion Research Center, King Abdullah University of Science and Technology (KAUST), Thuwal 23955-6900, Saudi Arabia
Email: hong.im@kaust.edu.sa

Colloquium 5: Turbulent Flames (Turbulent-Premixed)

Running title: Entrainment velocity in different regimes

Proc. Combust. Inst. 38, 2020, Abstract: 298

Word count (MS word): **TOTAL:** 6195.72 (MS-Word)

Words of text: 3621
Figures: 1862.6
Tables: 60.8
Equations: 144.4
References: 506.92

No figure needs to be printed in colour in the hard copy. All figures need to be printed in colour in the online version.

* Corresponding author

ABSTRACT

The statistics of entrainment velocity, defined as the displacement speed of an enstrophy isosurface, which can be taken to be the interface between turbulent/non-turbulent regions, have been analysed using a Direct Numerical Simulation database of statistically planar H_2-air flames with a range of different Karlovitz numbers. It has been found that the component of the entrainment velocity arising from molecular dissipation plays a leading order role for all values of Karlovitz number, whereas the relative importance of the baroclinic torque and dilatation rate weakens with increasing Karlovitz number. By contrast, the relative contribution of the entrainment velocity component arising from vortex-stretching strengthens with increasing Karlovitz number Ka. The mean entrainment velocity remains positive for the case representing the corrugated flamelets regime (i.e. $Ka < 1$), whereas it assumes negative values in the cases with large values of Karlovitz number (i.e. $Ka \gg 1$). The magnitude of the ratio of the mean values of entrainment velocity to the mean values of flame displacement speed conditional upon non-dimensional temperature within the flame front remains of the order of unity irrespective of Karlovitz number. However, the probability density functions of entrainment velocity exhibit considerably higher probabilities of finding large magnitudes than in the case of flame displacement speed. The alignments between the normal vector on the enstrophy isosurface and local principal strain rates have been found to be qualitatively similar to the corresponding alignments between flame normal and local principal strain rates, and the same holds true for the distributions of curvature shape factor of reaction progress variable and enstrophy isosurfaces. These findings indicate that the isosurface topologies and the alignments of normal vectors with local principal strain rates for enstrophy and reaction progress variable exhibit qualitatively similar behaviours. Consequently, turbulence and combustion modelling strategies cannot be considered in isolation in premixed turbulent flames.

Keywords: Enstrophy, entrainment velocity, displacement speed, baroclinic torque, curvature shape factor

1. INTRODUCTION

The interface between turbulent/non-turbulent (T/NT) fluid regions plays a key role in characterising the intermittency in turbulent flows [1,2]. Libby [3] proposed a transport equation for an intermittency function which varies from zero in the irrotational flow region to unity in the turbulent zone. This methodology has been revised by Dopazo [4,5] by associating physical mechanisms with the source terms of the intermittency function and linking them with the entrainment velocity, which is defined as the displacement speed of an enstrophy isosurface.

The enstrophy Ω is defined as $\Omega = \omega_i\omega_i/2$ where $\omega_i = \epsilon_{ijk}\partial u_k/\partial x_j$ and u_i are the ith components of vorticity and velocity, respectively. The speed at which an enstrophy isosurface moves normal to itself with respect to the local fluid velocity enables transition from the irrotational to the rotational region with an entrainment speed, which has the same magnitude but an opposite sign to that of the displacement speed for the enstrophy isosurface. In premixed flames, the T/NT interfaces and scalar isosurfaces are not coincident. Furthermore, in premixed combustion the flame surface moves normal to itself with respect to an initially coincident material surface with a displacement speed, so that fresh mixtures are engulfed into the flame with a velocity with same magnitude as that of the displacement speed. As such, the relative behaviours of entrainment velocity and flame displacement speed are of fundamental importance as they play key roles in the turbulent premixed flame stabilisation and flame anchoring events. Cifuentes et al. [6] analysed different components of entrainment velocity arising from different physical mechanisms for a flame-resolved simulation database for a bluff body stabilised flame, with the conditions ranging from the corrugated flamelets (CF) to the thin reaction zone (TRZ) regimes [7]. They found that the magnitudes of entrainment speed and displacement speed were comparable but the mean flame displacement speed was found to have positive values (i.e. flame propagating into unburned reactants), whereas the mean entrainment speed was reported to be negative indicating the entrainment of hot product into the reactants stream in that configuration. It is of interest to assess whether such findings are valid for a large range of Karlovitz number Ka values. Moreover,

the dominant physical mechanisms contributing to the entrainment speed variations need to be investigated at different Karlovitz numbers.

The present analysis addresses these fundamental questions by analysing a Direct Numerical Simulation (DNS) database of statistically planar turbulent H_2-air premixed flames considering detailed chemistry and transport, with turbulence parameters spanning a range of different Ka. The objectives of the current analysis are to identify the dominant physical mechanisms contributing to the entrainment velocity V_Ω, and its relative magnitude with respect to flame displacement speed S_d for different values of Ka along with the discussion on the implications of these findings.

2. MATHEMATICAL BACKGROUND AND NUMERICAL IMPLEMENTATION

The enstrophy Ω (i.e. $\Omega = \omega_i\omega_i/2$) transport equation takes the following form [8-10]:

$$\frac{\partial \Omega}{\partial t} + u_k \frac{\partial \Omega}{\partial x_k} = \underbrace{\omega_i \omega_k \frac{\partial u_i}{\partial x_k}}_{T_I} \quad \underbrace{-\epsilon_{ijk}\omega_i \frac{1}{\rho^2}\frac{\partial \rho}{\partial x_j}\frac{\partial \tau_{kl}}{\partial x_l}}_{T_{II}} + \underbrace{\frac{\epsilon_{ijk}\omega_i}{\rho}\frac{\partial^2 \tau_{kl}}{\partial x_j \partial x_l}}_{T_{III}} \quad \underbrace{-2\frac{\partial u_k}{\partial x_k}\Omega}_{T_{IV}} \quad + \underbrace{\epsilon_{ijk}\frac{\omega_i}{\rho^2}\frac{\partial \rho}{\partial x_j}\frac{\partial p}{\partial x_k}}_{T_V} \tag{1}$$

where $\tau_{kl} = \mu(\partial u_k/\partial x_l + \partial u_l/\partial x_k) - 2(\mu/3)\delta_{kl}(\partial u_m/\partial x_m)$ is the component of the viscous stress tensor, ρ is density and p is the pressure. Term T_I is the vortex stretching contribution to the enstrophy Ω transport, whereas term T_{II} arises due to misalignment between gradients of density and viscous stresses. Term T_{III} is responsible for molecular diffusion and dissipation of enstrophy Ω due to viscous action, whereas term T_{IV} represents the dilatation contribution. Term T_V is the baroclinic torque which arises due to misalignment between pressure and density gradients. For a given enstrophy Ω isosurface moving with a propagation velocity $\vec{v}_\Omega = \vec{u} + V_\Omega \vec{N}_\Omega$, eq. 1 can be written in the kinematic form for an iso-enstrophy surface as [6]:

$$\partial\Omega/\partial t + u_k\, \partial\Omega/\partial x_k = V_\Omega|\nabla\Omega| \tag{2}$$

where $\vec{N}_\Omega = -\nabla\Omega/|\nabla\Omega|$ is the vector on the iso-enstrophy surface. Comparing eqs. 1 and 2 yields the expression for the entrainment velocity V_Ω [6]:

$$V_\Omega = \underbrace{T_I/|\nabla\Omega|}_{V_1} + \underbrace{T_{II}/|\nabla\Omega|}_{V_2} + \underbrace{T_{III}/|\nabla\Omega|}_{V_3} + \underbrace{T_{IV}/|\nabla\Omega|}_{V_4} + \underbrace{T_5/|\nabla\Omega|}_{V_5} \tag{3}$$

Equation 3 provides the expression for the entrainment velocity V_Ω of an instantaneous enstrophy isosurface, as analysed by Cifuentes et al. [6] in the past.

The scalar fields in premixed flames are often characterized by a reaction progress variable $c = (Y_{\alpha 0} - Y_\alpha)/(Y_{\alpha 0} - Y_{\alpha\infty})$ and a non-dimensional temperature $\theta = (\tau - \tau_0)/(\tau_{ad} - \tau_0)$ where Y_α is the mass fraction of a suitable species α that varies monotonically across the flame, and τ, τ_0 and τ_{ad} are the instantaneous temperature, unburned gas temperature and adiabatic flame temperature, respectively. The transport equation of c is given by [7]: $\rho[\partial c/\partial t + \vec{u} \cdot \nabla c] = \nabla \cdot (\rho D \nabla c) + \dot{\omega}_c$ where $\dot{\omega}_c = -\dot{\omega}_\alpha/(Y_{\alpha 0} - Y_{\alpha\infty})$ is the reaction rate of c with $\dot{\omega}_\alpha$ being the reaction rate of species α. The isosurfaces of c propagate with a propagation speed $\vec{v}_c = \vec{u} + S_d\vec{N}$ where S_d is the flame displacement speed and $\vec{N} = -\nabla c/|\nabla c|$ is the flame normal vector pointing towards the unburned gas. Accordingly, the flame displacement speed S_d for a given c isosurface [11,12] can be derived as:

$$S_d = \underbrace{\dot{\omega}_c/\rho|\nabla c|}_{S_r} + \underbrace{\vec{N} \cdot \nabla\left(\rho D \vec{N} \cdot \nabla c\right)/\rho|\nabla c|}_{S_n} \underbrace{-2D\kappa_m}_{S_t} \quad (4)$$

where S_r, S_n and S_t are the reaction, normal diffusion and tangential diffusion components of displacement speed and $\kappa_m = 0.5\nabla \cdot \vec{N}$ is the local flame curvature. Here, the statistics of S_d and its components are shown for $\alpha = H_2, O_2$ and H_2O.

A DNS database [9,13] of statistically planar H_2-air flames with an equivalence ratio of 0.7 is considered. For this equivalence ratio H_2-air flames remain thermo-diffusively neutral in terms of stretch rate dependence [14]. A detailed chemical mechanism [15] involving 9 species and 19 chemical reactions is used for this analysis. For this database, the unburned gas temperature τ_0 is at 300K and pressure is atmospheric, which yields an unstrained laminar burning velocity $S_L = 135.62\text{cm/s}$. A pre-computed divergence free, homogeneous, isotropic turbulence field is injected through the inlet. The mean inlet velocity has been gradually modified to match turbulent flame speed during the simulation and the flame is considered to be statistically stationary when the flame area does not vary with time [9]. Turbulent inflow and outflow boundaries are specified in the direction of mean flame propagation

and transverse boundaries are considered to be periodic. The inlet values of normalised root-mean-square turbulent velocity fluctuation u'/S_L , turbulent length scale to flame thickness ratio l_T/δ_{th}, Damköhler number $Da = l_T S_L/u'\delta_{th}$, Karlovitz number $Ka = (\rho_0 S_L \delta_{th}/\mu_0)^{0.5}(u'/S_L)^{1.5}(l_T/\delta_{th})^{-0.5}$ and turbulent Reynolds number $Re_t = \rho_0 u' l_T/\mu_0$ for all cases are provided in Table 1, where ρ_0 is the unburned gas density, μ_0 is the unburned gas viscosity, l_T is the most energetic length scale, $\delta_{th} = (\tau_{ad} - \tau_0)/\max|\nabla\tau|_L$ is the thermal flame thickness for the 1D steady unstretched laminar premixed flame. Cases A and B represent the CF ($Ka < 1$) and TRZ ($1 < Ka < 100$) regimes of combustion and according to the regime diagram by Peters [16] case C belongs to the Broken Reaction Zones (BRZ) regime ($Ka > 100$). If the BRZ regime combustion is realised in case C in the true sense is not relevant to this analysis, but without doubt cases A-C represent a sufficiently wide spectrum of flame characteristics in the Ka space to provide valuable insights into the change in the dominant physical processes. The domain size is taken to be $20mm \times 10mm \times 10mm$ ($8mm \times 2mm \times 2mm$) in cases A and B (case C) and the domain has been discretised by a uniform Cartesian grid of $512 \times 256 \times 256$ ($1280 \times 320 \times 320$) ensuring resolution of the flame and the Kolmogorov length scale. Simulations have been conducted for $1.0t_e$, $6.8t_e$ and $6.7t_e$ (i.e. $t_e = l_T/u'$) for cases A-C, respectively, by which the flame surface area and turbulent flame speed reached a quasi-stationary state and a detailed discussion in this regard can be found elsewhere [13]. The longitudinal integral scale L_{11} is a factor of 2.5 smaller than most energetic scale l_T for these cases and thus the simulation time is $\{2.5,17,16.75\}L_{11}/u'$ for cases A-C, respectively. The values of Ka (Da) in Table 1 increase (decrease) by a factor 1.6 (2.5) if L_{11} instead of l_T is used for their definitions.

The left and right sides of eq. 1 have been evaluated separately and the maximum difference has been found to be smaller than 1% for the postprocessing methods adopted here. A number of snapshots were used after the quasi-stationary state is obtained for the statistical analysis presented in this paper. These statistics remain qualitatively valid since halfway of the simulation time.

Table 1:

List of inflow turbulence parameters

Case	u'/S_L	l_T/δ_{th}	Re_t	Da	Ka
A	0.7	14.0	227	20.0	0.75
B	5.0	14.0	1623	2.8	14.4
C	14.0	4.0	1298	0.29	126

3. RESULTS & DISCUSSION

The distributions of log $(\Omega \times \delta_{th}^2/S_L^2)$ in the central mid-plane for cases A-C are presented in Figs. 1a-c (not in same scale). Figures 1a-c reveal that the frequencies of the occurrences of large magnitudes in Ω increase from case A to case C as Ka increases. It is further seen that the enstrophy level increases across the flame for case A, whereas it drops drastically from the unburned to the burned gas side in cases B and C.

Figure 2 shows the mean values of $\Omega \times \delta_{th}^2/S_L^2$ conditional on θ for cases A-C. In case A, the mean Ω increases significantly across the flame and decreases far downstream, whereas case C demonstrates a monotonic drop in the mean Ω from the unburned to the burned gas side. In case B, the mean Ω decreases initially but exhibits some moderate increase within the flame before eventually decaying on the burned gas side. The flame-generated vorticity due to T_V is primarily responsible for the augmentation of Ω across the flame in case A [10]. By contrast, T_{III} and T_{IV} are principally responsible for the decay of Ω from the unburned to the burned gas side of the flame in case C [10]. Although T_{III} and T_{IV} act to decay the enstrophy in case B, T_I and T_V contributions tend to generate Ω within the flame and thus case B exhibits a trend which is somewhat in between the behaviours shown by cases A and C. The mean behaviours of $T_I, T_{II}, T_{III}, T_{IV}$ and T_V for this database have been reported elsewhere [10] and thus are not repeated here but interested readers are referred to Ref. [10] for further information.

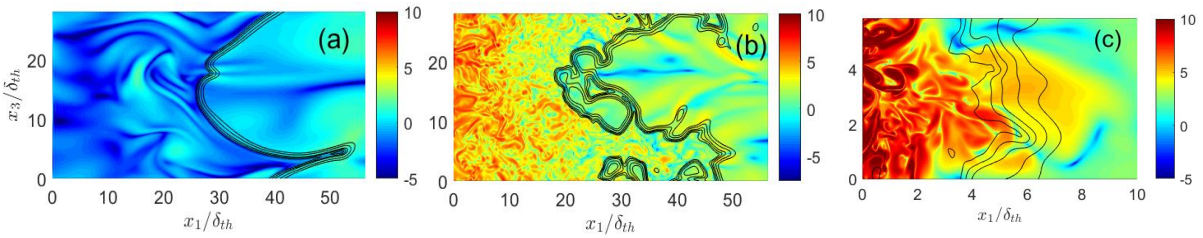

Fig. 1: Distributions of natural logarithm of normalised enstrophy log $(\Omega \times \delta_{th}^2/S_L^2)$ in the central mid-plane for (a-c) cases A-C. The contours of $\theta = 0.1, 0.3, 0.5, 0.7$ and 0.8 (from left to right) are shown by black lines. Note the different scale and magnified view for case C.

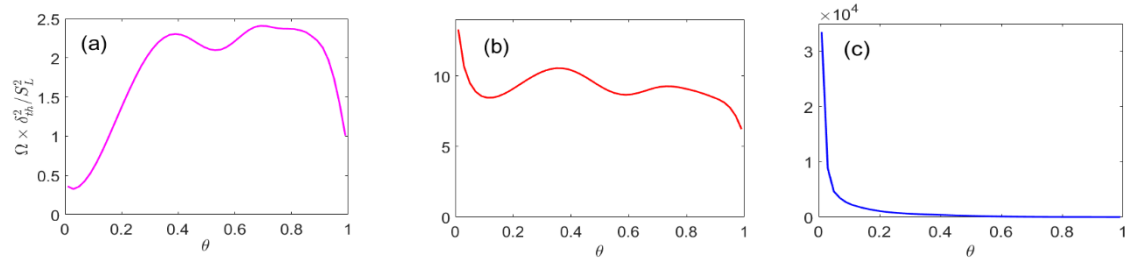

Fig. 2: Variations of the mean values of normalised enstrophy $\Omega \times \delta_{th}^2/S_L^2$ conditional upon θ for (a-c) cases A-C.

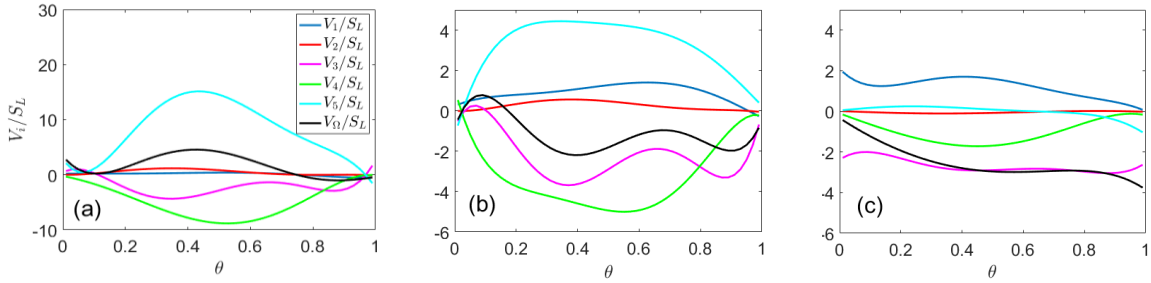

Fig. 3: Variations of the mean values of V_Ω/S_L and its components (i.e. V_i/S_L where $i = 1, 2, 3, 4, 5$) conditional on θ for (a-c) cases A-C.

The variations of the mean values of V_Ω/S_L and its components (i.e. V_i/S_L where $i = 1,2,3,4,5$) conditional on θ for cases A-C are shown in Figs. 3a-c. The mean value of V_Ω is overall positive in case A, implying that the T/NT interface propagates from the higher vorticity to the lower vorticity region. As Ka increases in cases B and C, the mean V_Ω becomes negative, implying that the T/NT interface retreats into the high vorticity region. Considering mean Ω variations shown in Fig. 2, the T/NT interface moves toward the unburned gas side from the burned gas side. However, the underlying mechanisms behind the forward propagation of T/NT interface may be significantly different.

To understand this further, the individual components V_i/S_L are examined. Figure 3a shows that the positive mean entrainment speed in case A is mainly driven by the baroclinic torque (V_5), which overrides the retreating effect of the viscous dissipation (V_3) and dilatation (V_4) terms. The vortex-stretching (V_1) and the density and stress tensor gradient misalignment (V_2) have negligible effect here. On the other hand, in case C the negative entrainment speed mainly follows the viscous dissipation (V_3) and dilatation (V_4), which is slightly offset by the positive vortex-stretching effect (V_1) which is expected for the strong turbulence level. Case B falls in between, where the retreating negative entrainment speed is mainly due to the V_3 and V_4 as in case C, while a significant level of flame-generated vorticity promotes positive V_Ω and attenuates the magnitude of the retreatment. In summary, in the flamelet regime the T/NT interface behavior is dominated by the flame-generated vorticity, while the effects become attenuated at high Ka and the usual characteristics of non-reacting turbulence are recovered.

Figure 4 shows the variations of the mean values of S_d/S_L and its components (i.e. S_r/S_L , S_n/S_L and S_t/S_L) conditional on θ, in cases A to C. The results are not shown for $\theta < 0.1$ and $\theta > 0.9$ in order to avoid numerical noise introduced by vanishingly small values of $|\nabla c|$ (see eq. 4). The mean value of S_d increases from the unburned to the burned gas side due to density drop caused by heat release. The mean value of S_r remains positive throughout the flame, whereas the mean value of S_n assumes positive values towards the unburned gas side and negative values in the burned gas side for all choices of c. The mean value of S_t remains negligible due to small mean curvature values in the statistically planar flames. To verify that the results do not depend on the choice of the progress variable, S_d was computed for c based on H_2, O_2 and H_2O mass fractions and the results are overlaid in Fig. 4. Although there are some quantitative differences, the key conclusions remain consistent regardless of the choice of c. The quantitative differences of S_d for c based on different species mass fractions are consistent with previous DNS results by Wang et al. [17]. Figures 3a-c indicate that the mean value of V_Ω can assume both positive and negative values but the mean value of S_d conditional upon θ remains positive for all cases (see Figs. 4a-c), as expected in propagating premixed flames. Figures 3 and 4 suggest that

chemical reaction affects V_5 arising from the baroclinic torque and displacement speed through its reaction component S_r and thus an analysis based on a non-reacting mixing layer with density variation is unlikely to offer accurate insights into the entrainment velocity and displacement speed behaviours expected from premixed flames.

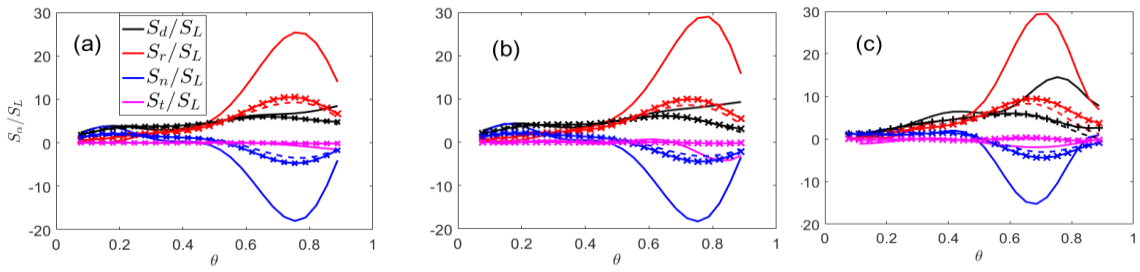

Fig. 4: Variations of the mean values of S_d/S_L and its components (i.e. S_r/S_L, S_n/S_L and S_t/S_L) conditional on θ for c definitions based on H_2, O_2 and H_2O mass fractions (solid line, broken line, and line with crosses, respectively) for (a-c) cases A-C.

Note that V_Ω and S_d are uncorrelated and it was claimed that their mean values are of the same order for $Ka \approx 1.0$ in Ref. [6] and thus it is worth assessing if this remains valid for other conditions in terms of Ka. Therefore, the ratio $R_{\Omega d}$ of the mean values of V_Ω and S_d (i.e. $R_{\Omega d} = \langle V_\Omega|\theta\rangle/\langle S_d|\theta\rangle$) across the flame for cases A-C is shown in Fig. 5a. It can be seen from Fig. 5a that the magnitude of $R_{\Omega d}$ remains at order unity but the value is positive for case A, whereas it is negative for cases B and C. Again, the results based on different definitions of c are shown in Fig. 5a with consistent behaviour. The probability density functions (PDFs) of V_Ω/S_L and S_d/S_L are shown in Figs. 5b-d for $\theta = 0.7$ in cases A-C where c was defined based on H_2O mass fraction. Figures 5b-d indicate that V_Ω/S_L shows higher probability of finding large magnitudes of both positive and negative values than in the case of S_d/S_L. The probability of finding negative value of S_d/S_L is zero in cases A and B on $\theta = 0.7$ isosurface but a small probability of finding negative S_d/S_L is observed for case C. This is found to be consistent with previous DNS results [18] and scaling arguments [7]. The variations of the S_d/S_L PDFs in response to the changes in u'/S_L and Ka have been discussed elsewhere [18,19] and will not be repeated here. Figures 5b-d show that the PDFs of V_Ω on $\theta = 0.7$ isosurface peak at a negative value and the PDF of V_Ω is skewed towards the negative value in case C but this trend is not prominent in cases A and B.

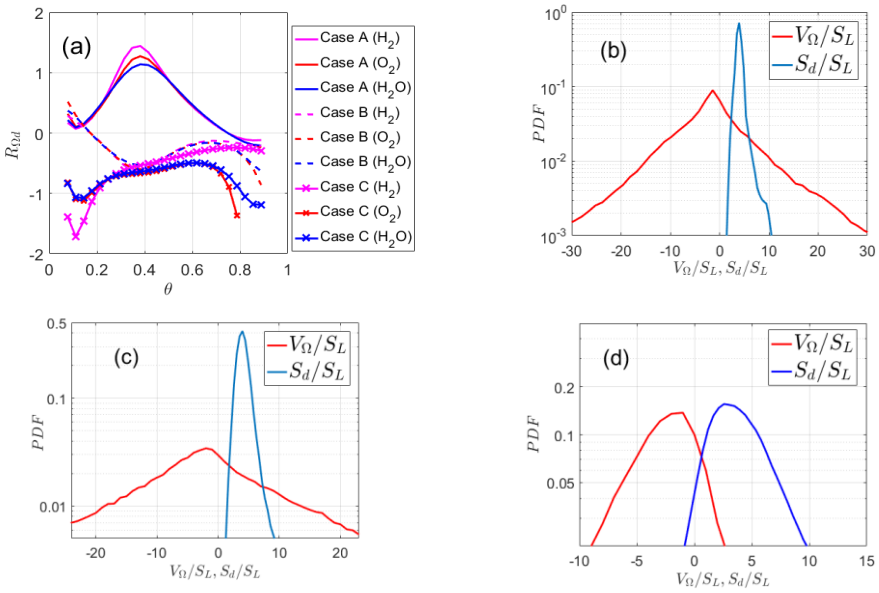

Fig. 5: (a) Variations of the ratio $R_{\Omega d}$ of mean values of V_Ω and S_d (i.e. $R_{\Omega d} = \langle V_\Omega|\theta\rangle/\langle S_d|\theta\rangle$) conditional on θ for c definitions based on H_2, O_2 and H_2O mass fractions and (b-d) PDFs of V_Ω/S_L and S_d/S_L (in logarithmic scale) for $\theta = 0.7$ for c definition based on H_2O mass fraction for cases A-C.

The findings from Figs. 5b-d indicate that the distributions of V_Ω and S_d are significantly different although the mean values of V_Ω and S_d remain comparable and this is valid for all cases considered here irrespective of Ka and definition of c.

A combination of predominant Ω generation from the unburned to the burned gas side and positive mean values of V_Ω and S_d does not necessarily indicate that the directions of Ω entrainment and flame propagation are aligned with each other in case A. Similarly, a combination of positive mean S_d and negative mean V_Ω does not imply that the Ω entrainment and flame normal are collinearly orientated in the opposite direction. The alignment behaviour is analysed in detail by the variations of the mean values of $\Psi_\alpha = |\cos\alpha_c|$, $\Psi_\beta = |\cos\beta_c|$, $\Psi_\gamma = |\cos\gamma_c|$, $\Phi_\alpha = |\cos\alpha_\Omega|$, $\Phi_\beta = |\cos\beta_\Omega|$ and $\Phi_\gamma = |\cos\gamma_\Omega|$ conditional upon θ, which are presented in Figs. 6a-c for cases A-C, respectively, where α_c, β_c and γ_c ($\alpha_\Omega, \beta_\Omega$ and γ_Ω) are the angles between $\vec{N}$ ($\vec{N}_\Omega$) with the most extensive, intermediate and most compressive principal strain rates, respectively. The Ψ_α, Ψ_β, Ψ_γ, Φ_α, Φ_β and Φ_γ statistics presented in Figs. 6a-c are for c based on H_2O mass fraction only and other definitions of c yielded similar results.

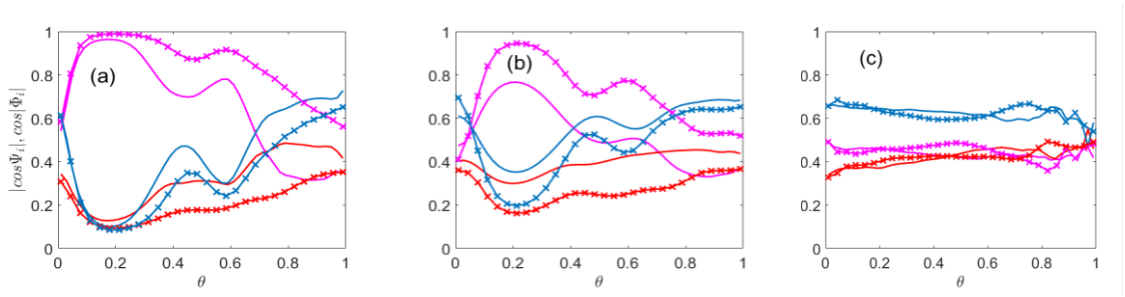

Fig. 6: Mean values of $\Phi_\alpha = |\cos\alpha_\Omega|$ (magenta solid line), $\Phi_\beta = |\cos\beta_\Omega|$ (red solid line) and $\Phi_\gamma = |\cos\gamma_\Omega|$ (blue solid line), $\Psi_\alpha = |\cos\alpha_c|$ (magenta line with crosses), $\Psi_\beta = |\cos\beta_c|$ (red line with crosses) and $\Psi_\gamma = |\cos\gamma_c|$ (blue line with crosses) conditional upon θ for (a-c) cases A-C.

Figure 6 shows that the mean value of Φ_α (Ψ_α) remains greater than the mean values of Φ_β and Φ_γ (Ψ_β and Ψ_γ) for the major part of the flame in case A but this behaviour changes towards the burned gas side where the effects of thermal expansion are weak and the mean value of Φ_γ (Ψ_γ) assumes the highest value. In cases A and B, the mean value of Φ_α (Ψ_α) assumes greater magnitudes than those of Φ_β and Φ_γ (Ψ_β and Ψ_γ) around $0.1 \leq \theta \leq 0.3$ where the dilatation rate effects are the strongest in these flames [20], whereas the mean value of $\Phi_\gamma(\Psi_\gamma)$ remains greater than those of Φ_α and Φ_β (Ψ_α and Ψ_β) for the major part of the flame in case C. This suggests that $\vec{N}$ and $\vec{N}_\Omega$ predominantly align with the eigenvector corresponding to the most extensive principal strain rate in case A and only in the region where thermal expansion effects are strong in cases B and C, whereas $\vec{N}$ and $\vec{N}_\Omega$ preferentially align collinearly with the most compressive principal strain rate direction for the major part of the flame in cases B and C, and also in the burned gas side in case A. It has been discussed elsewhere that $\vec{N}$ preferentially aligns with the most extensive principal strain rate for $Da \gg 1$ [21] and also in the region where the strain rate induced by thermal expansion dominates over turbulent straining even for $Da < 1$. By contrast, $\vec{N}$ preferentially aligns with the most compressive principal strain rate similar to passive scalar mixing [22], when turbulent straining dominates over the strain rate induced by thermal expansion [21]. The findings from Fig. 6 suggest that $\vec{N}_\Omega$ behaves similar to $\vec{N}$ and they are collinearly aligned. It is important to note that vorticity $\vec{\omega}$ predominantly aligns with the intermediate principal

strain rate for all cases (not shown here but consistent with Refs. [22,23]) but the alignment of $\vec{N}_\Omega$ (where $N_{\Omega i} = -\omega_i \partial\omega_i/\partial x_j \, /|\nabla\Omega|$) is not only dependent on ω_i but also on $\partial\omega_i/\partial x_j$ and $|\nabla\Omega|$.

Finally, differences in the topologies of c and Ω isosurfaces are examined. The PDFs of curvature shape factors $s_{h\Omega}$ and s_{hc} for c (based on H_2O mass fraction but other definitions yielded similar results) and Ω isosurfaces for $\theta = 0.3, 0.5$ and 0.7 isosurfaces are shown in Fig. 7. The curvature shape factor for an isosurface is defined as $\kappa_{min}/\kappa_{max}$, which is calculated from the two principal curvatures κ_1 and κ_2 of the isosurface [24,25] such that κ_{min} is the smaller of κ_1 and κ_2 by magnitude and κ_{max} is the other. The shape factors $s_{h\Omega} = 1.0$ and $s_{hc} = 1.0$ correspond to spherical curvatures, whereas $s_{h\Omega} = -1.0$ and $s_{hc} = -1.0$ indicate spherical saddle points. The shape factors of $s_{h\Omega} = 0.0$ and $s_{hc} = 0.0$ correspond to locally cylindrical two-dimensional surfaces. The joint PDFs of $= 0.5(\kappa_1 + \kappa_2)$ and Gauss curvature $\kappa_1\kappa_2$ for both c and Ω isosurfaces have been found to be qualitatively similar to that presented in Cifuentes et al. [6] and thus are not repeated here.

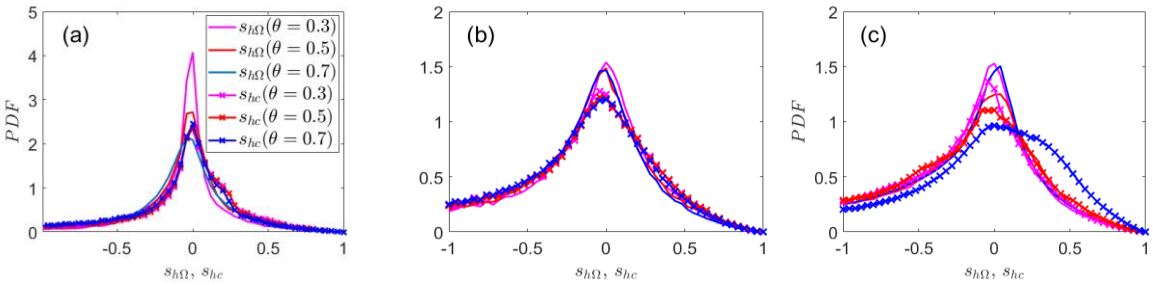

Fig. 7: PDFs of curvature shape factors $s_{h\Omega}$ and s_{hc} for $\theta = 0.3, 0.5$ and 0.7 isosurfaces for (a-c) cases A-C.

Figure 7 shows that the probability of finding a local cylindrical structure is the highest for both c and Ω isosurfaces. There is a modest probability of finding saddle points and zero probability of finding spherical curvature on both c and Ω isosurfaces for all cases considered here. Figures 7a-c reveal that the probability of saddle type topologies for both c and Ω isosurfaces increases from case A to case C. Figure 7 shows that there are little variations in the PDFs of $s_{h\Omega}$ and s_{hc} between different θ for all cases considered here.

The findings from Figs. 5-7 indicate that the topologies of c and Ω isosurfaces remain qualitatively similar and $\vec{N}$ and $\vec{N}_\Omega$ remain collinearly aligned for all cases considered here. Thus, turbulence and combustion modelling strategies cannot be considered in isolation in premixed turbulent flames and both turbulence and combustion modelling strategies should account for the variation of Ka for accurate modelling of premixed turbulent flames. This is also reflected in the modelling of turbulent scalar fluxes and sub-grid stresses, as indicated in [26,27].

4. CONCLUSIONS

The statistics of V_Ω and S_d and their components have been analysed based on a DNS database of statistically planar turbulent H_2-air flames with an equivalence ratio of 0.7 with a range of different Ka. It has been found that baroclinic torque and dilatation rate components of V_Ω play key roles for the flame with $Ka < 1$ but their influences weaken progressively with increasing Ka. By contrast, the relative contribution of the vortex-stretching component of V_Ω strengthens with increasing Ka. The statistical behaviours of S_d and its components have been shown to be qualitatively similar in flames of different values of Ka. However, the individual components of S_d have been found to be affected by the definition of c. In the flame with $Ka < 1$, the mean V_Ω remains positive but it assumes negative values in the flames representing $Ka > 1$. The ratio of mean values of V_Ω and S_d conditioned on non-dimensional temperature remains of the order of unity but the PDFs of V_Ω exhibit higher probabilities of finding large magnitudes than those in the case of S_d. The isosurfaces of c and Ω have been shown to exhibit qualitatively similar surface topologies and the corresponding normal vectors also show qualitatively similar alignments with local principal directions, which change with $Da \sim Re_t^{0.5}/Ka$. These findings suggest that it is not only sufficient to modify the mean reaction rate closure with the variation of Ka but an alternation of the underlying turbulence modelling might also be necessary for accurate predictions of turbulent premixed combustion. The cases considered in the present study indicate clear trends in terms of statistical behaviours of V_Ω and topologies of c and Ω isosurfaces with

increasing Ka but more cases need to be investigated to identify the dominant physical processes in different combustion regimes.

ACKNOWLEDGEMENTS

NC is grateful to EPSRC (EP/K025163/1, EP/R029369/1) and ARCHER for computational support. HGI is grateful to KAUST for research funding and computational support respectively.

REFERENCES

[1] S. Corrsin, Investigation of flow in an axially symmetrical heated jet of air, NACA Report No. W-94, 1943.

[2] S. Corrsin, A. Kistler, Free-stream boundaries of turbulent flows, NACA Report No. 1244 , 1955.

[3] P.A. Libby, On the prediction of intermittent turbulent flows, J. Fluid Mech., 68 (1975) 273–295.

[4] C. Dopazo, On conditioned averages for intermittent turbulent flows, J. Fluid Mech., 81 (1977) 433–438.

[5] C. Dopazo, A probabilistic approach to turbulent flame theory, Acta Astron., 6 (1977) 999–1004.

[6] L. Cifuentes, A. M. Kempf, C. Dopazo, Local entrainment velocity in a premixed turbulent annular jet flame, Proc. Combust. Inst., 37 (2019) 2493-2501.

[7] N. Peters, P. Terhoeven, J.H. Chen, T. Echekki, Proc. Combust. Inst., 27 (1998) 833-839.

[8] N. Chakraborty, I. Konstantinou, A. Lipatnikov, Effects of Lewis number on vorticity and enstrophy transport in turbulent premixed flames, Phys. Fluids 28 (2016) 015109.

[9] C. Dopazo, L. Cifuentes, N. Chakraborty, Vorticity budgets in premixed combusting turbulent flows at different Lewis numbers, Phys. Fluids 29 (2017) 045106.

[10] V. Papapostolou, D. H Wacks, M. Klein, N. Chakraborty, H. G. Im, Enstrophy transport conditional on local flow topologies in different regimes of premixed turbulent combustion, Scientific Reports, 7 (2017) 11545.

[11] T. Echekki, J.H. Chen, Analysis of the contribution of curvature to premixed flame propagation Combust. Flame 118 (1999) 308–311.

[12] N. Chakraborty, S. Cant, Unsteady effects of strain rate and curvature on turbulent premixed flames in an inflow-outflow configuration, Combust. Flame 137 (2004) 129–147.

[13] H.G. Im, P.G. Arias., S. Chaudhuri, H.A. Uranakara, Direct numerical simulations of statistically stationary turbulent premixed flames, Combust. Sci. Technol., 188 (2016) 1182-1198.

[14] J. H. Chen, H.G. Im, Correlation of flame speed with stretch in turbulent premixed Methane/Air flames, Proc. Combut. Inst., Pittsburgh, 27 (1998) 819-826.

[15] M.P. Burke, M. Chaos, Y. Ju, F.L. Dryer, S.J. Klippenstein, Comprehensive H2-O2 kinetic model for high-pressure combustion, Int. J. Chem. Kin., 44, (2012) 444-474.

[16] N. Peters, Turbulent Combustion, Cambridge University Press, 2000.

[17] H. Wang, E.R. Hawkes, J. H. Chen, A direct numerical simulation study of flame structure and stabilization of an experimental high Ka CH4/air premixed jet flame, Combust. Flame, 180 (2017) 110-123.

[18] N. Chakraborty, Comparison of displacement speed statistics of turbulent premixed flames in the regimes representing combustion in corrugated flamelets and thin reaction zones, Phys. Fluids, 19 (2007) 105109.

[19] N. Chakraborty, M. Klein, R.S. Cant, Effects of turbulent Reynolds number on the displacement speed statistics in the thin reaction zones regime turbulent premixed combustion, J. Combust., 2011 (2011) 473679.

[20] D.H. Wacks, N. Chakraborty, M. Klein, P.G. Arias, H.G. Im, Flow topologies in different regimes of premixed turbulent combustion: A direct numerical simulation analysis, Phys. Rev. F, 1, (2016) 083401.

[21] N. Chakraborty, N. Swaminathan, Influence of Damköhler number on turbulence-scalar interaction in premixed flames, Part I: Physical Insight , Phys. Fluids, 19 (2007) 045103.

[22] W.T. Ashurst, A. Kerstein, R.M. Kerr, C.H. Gibson, Numerical simulation of turbulent flame structure with non-unity Lewis number, Phys. Fluids A, 30 (1987) 2343.

[23] N. Chakraborty, Alignment of vorticity with strain rates in turbulent premixed flames, Eur. J. Mech. B-Fluids, 46 (2014) 201-220.

[24] R.S. Cant, C.J. Rutland, A. Trouvé, Statistics for laminar flamelet modelling, Proceeding of the Summer Program 1990, Center for Turbulence Research, Stanford, pp. 271-279, 1990.

[25] C. Dopazo , J. Martin , J. Hierro, Local geometry of isoscalar surfaces, Phys. Rev. E. 76 (2007) 056316.

[26] M. Klein, C. Kasten, N. Chakraborty and Y. Gao, A-priori Direct Numerical Simulation assessment of sub-grid scale stress tensor closures for turbulent premixed combustion, Comp. Fluids, 122 (2015) 1-11.

[27] M. Klein, C. Kasten, N. Chakraborty, N. Mukhadiyev and H.G. Im, Turbulent scalar fluxes in Hydrogen-Air premixed flames at low and high Karlovitz numbers, Combust. Theor. Modell., 22 (2018) 1-16.

FIGURE CAPTIONS

Fig. 1: Distributions of natural logarithm of normalised enstrophy log $(\Omega \times \delta_{th}^2/S_L^2)$ in the central mid-plane for (a-c) cases A-C. The contours of $\theta = 0.1,0.3,0.5,0.7$ and 0.8 (from left to right) are shown by black lines. Note the different scale and magnified view for case C.

Fig. 2: Variations of the mean values of normalised enstrophy $\Omega \times \delta_{th}^2/S_L^2$ conditional on θ for (a-c) cases A-C.

Fig. 3: Variations of the mean values of V_Ω/S_L and its components (i.e. V_i/S_L where $i = 1,2,3,4,5$) conditional on θ for (a-c) cases A-C.

Fig. 4: Variations of the mean values of S_d/S_L and its components (i.e. S_r/S_L , S_n/S_L and S_t/S_L) conditional on θ for c definitions based on H_2, O_2 and H_2O mass fractions (solid line, broken line, and line with crosses, respectively) for (a-c) cases A-C.

Fig. 5: (a) Variations of the ratio $R_{\Omega d}$ of mean values of V_Ω and S_d (i.e. $R_{\Omega d} = \langle V_\Omega|\theta\rangle/\langle S_\mathrm{d}|\theta\rangle$) conditional on θ for c definitions based on H_2, O_2 and H_2O mass fractions and (b-d) PDFs of V_Ω/S_L and S_d/S_L (in logarithmic scale) for $\theta = 0.7$ for c definition based on H_2O mass fraction for cases A-C.

Fig. 6: Mean values of $\Phi_\alpha = |\cos\alpha_\Omega|$ (magenta solid line), $\Phi_\beta = |\cos\beta_\Omega|$ (red solid line) and $\Phi_\gamma = |\cos\gamma_\Omega|$ (blue solid line), $\Psi_\alpha = |\cos\alpha_c|$ (magenta line with crosses), $\Psi_\beta = |\cos\beta_c|$ (red line with crosses) and $\Psi_\gamma = |\cos\gamma_c|$ (blue line with crosses) conditional upon θ for (a-c) cases A-C.

Fig. 7: PDFs of curvature shape factors $s_{h\Omega}$ and s_{hc} for $\theta = 0.3, 0.5$ and 0.7 isosurfaces for (a-c) cases A-C.